scientific reports

Check for updates

OPEN

Towards definitive functional forms for Monin–Obukhov similarity functions in stable and very stable surface layers

G. Casasanta[1], M. Conte[1]✉, R. Sozzi[2], A. Cecilia[1], I. Petenko[1] & S. Argentini[1]

Monin–Obukhov similarity functions are key components in all numerical models of atmospheric flows, yet their exact functional forms remain a matter of debate. Existing formulations, typically derived through empirical curve fitting, often result in inconsistencies and physically questionable behaviour, particularly under stable and very stable conditions. This paper bridges the well-established Monin–Obukhov Similarity Theory (MOST) with the more recent Energy and Flux Budget (EFB) second-order closure to analytically derive the functional forms of all MOST similarity functions under stable conditions. In addition, it identifies and formalises a set of constrain relationships that characterise the physical connection among the universal functions, highlighting their interdependences. Our results aim to advance the theoretical understanding of the stable surface layer and offer a pathway toward more physically grounded turbulence parameterizations, with implications for improving the performance of numerical weather prediction, air quality, ocean, and climate models.

List of symbols

A_i	Share of the TKE components ($i = x, y, z$)
C_i	EFB closure numerical constants ($i = 0, 1, 2, F, P, r, \tau$)
C_{V^2}	Structure function parameters for velocity
C_{T^2}	Structure function parameters for temperature
E	Total turbulent energy
E_i	Longitudinal ($i = x$), transverse ($i = y$) and vertical ($i = z$) components of E_k
E_{int}	Inter-component energy exchange TKE
E_k	Turbulent kinetic energy (TKE)
E_p	Turbulent potential energy (TPE)
E_θ	Potential temperature fluctuation energy
$\Im_i$	EFB universal functions ($i = Ri, Ri_E, Ri_{Ex}, Ri_{Ey}, Ri_{Ez}, Ri_f, Pr_T, w\theta, \tau, \tau x, \tau y, \tau z$)
g	Acceleration due to gravity
k	Von Kármán constant
L	Obukhov length scale
t_T	Turbulence time scale
u', v', w'	Wind velocity fluctuation components
u_*	Friction velocity
$\underline{U}, \underline{V}, \underline{W}$	Mean wind velocity components
$\overline{u'w'}, \overline{v'w'}$	Reynold stress components
$\overline{w'\theta'}$	Kinematic heat flux
Pr_T	Turbulent Prandtl Number
Q_{zz}	Inter-component energy exchange term
Ri	Richardson Number
Ri_E	Energy Richardson Number
Ri_{Ex}, Ri_{Ey}	Longitudinal and transverse Energy Richardson Number
Ri_f	Flux Richardson Number
R_∞	Asymptotic limit of Ri_f

[1]Institute of Atmospheric Sciences and Climate (CNR- ISAC), National Research Council of Italy, Rome, Italy. [2]Servizi e Territorio s.r.l, Milan, Italy. ✉email: m.conte@isac.cnr.it

T_*	Temperature scale
β	Buoyancy parameter
θ'	Potential temperature fluctuation
Θ	Mean potential temperature
$\varepsilon_K, \varepsilon_\theta$	Dissipation rates for E_k and E_θ
ζ	Stability parameter
σ_i	Wind component standard deviations ($i = u, v, w$)
τ	Friction velocity squared
Φ_m, Φ_h	Universal function for wind and temperature gradients
$\Phi_{uu}, \Phi_{vv}, \Phi_{ww}$	Universal functions for the standard deviation of wind velocity
$\Phi_{\theta\theta}$	Universal function for the standard deviation of potential temperature
$\Phi_{\varepsilon k}, \Phi_{C_{V^2}}, \Phi_{C_{T^2}}$	Universal function for ε_K, C_{V^2}, and C_{T^2}

Similarity functions are crucial components of the Monin-Obukhov similarity theory (MOST)[1], which is widely used in all numerical weather prediction (NWP), ocean, air pollution and climate models to parametrise the turbulent energy exchange between the atmosphere and the underlying surface[2,3]. Based on dimensional analysis, MOST was originally developed for flat and horizontally homogeneous terrain, considering a steady state surface layer (SL) unaffected by nonturbulent motions (paradigmatic conditions) and subsidence. Under both neutral and convective atmospheric conditions, vertical fluxes of momentum, sensible heat and passive scalars can be considered as quasi-constant with height (see, e.g[4]). , while an alternative scaling approach has been developed to include stable conditions (local similarity[5,6]), where vertical turbulent fluxes depend on height. Since local similarity is formally identical to MOST, except for considering turbulent fluxes at a specific height, the result presented in this paper applies to both approaches.

Under paradigmatic conditions, a single length scale L(the Obukhov length) is enough to characterise all the surface-atmosphere turbulent exchanges, so that any relevant variable x, nondimensionalized with respect to a proper turbulent scaling variable x_*, is expressed as a universal function $\Phi_x(\zeta)$ of the scaling parameter $\zeta = z/L$, where z is the height above the surface[7]. The functional forms of $\mathbf{\Phi}_x(\zeta)$ are not provided by MOST and have to be determined experimentally, usually through curve fitting. Especially under stable and very stable conditions, when mechanical turbulence tends to be suppressed by a strong thermal stratification, measurements are often perturbated by nonturbulent motions such as internal gravity waves, Kelvin-Helmholtz shear instability, low-level jets, meso and sub-meso motions[8–11]. In addition, the possible presence of self-correlations, which may seriously affect the regression analysis, is often neglected[12,13]. Such difficulties in performing accurate measurements under stable conditions may explain why the main formulations proposed in literature are not fully consistent with what we know of the stable SL phenomenology[14].

A completely different scheme to describe and forecast the SL state consists in applying an appropriate closure to the fluid mechanics Eqs.[6,7], an approach widely used in NWP and air quality models, most of which use one of the many available versions or extension of the famous Mellor-Yamada closure[15,16]. Also in this case, while a 40-year effort has led to an accurate and reliable description of the SL under convective conditions, stable cases have been difficult to address since the beginning[17]. Although this difficulty has been known for a long time, only in the last decades the availability of data from Arctic and Antarctic research stations, acquired under high and persistent stability conditions, has seriously questioned the reliability of the turbulence closure techniques implemented so far, leading to the need of new schemes, including recent machine learning-based approaches applied to fluid dynamics problems (e.g[18–22]). In particular, in the last 15 years Zilitinkevich and colleagues developed and refined the Energy and Flux Budget (EFB) second order closure, capable of addressing a number of stable and very stable SL characteristics, including the presence of a minimum in the sensible heat flux[23–29], the inter-component exchange of turbulent kinetic energy between vertical and horizontal components[30], the exchange of turbulent potential and kinetic energy[30], as well as the existence of a critical value for the Flux Richardson Number Ri_f but not for the Richardson Number Ri[30,31]. According to the detailed analysis reported in Li et al.[32], the second order EFB closure currently provides the most realistic fluid-dynamic representation of the SL under stable and strongly stable conditions.

To the best of our knowledge, little effort has been made to harmonise MOST with the governing equations for turbulent flow, if not limited to Mellor Yamada closure[33,34]. Nevertheless, despite the critical limitation represented by the absence of a convincing and generally accepted description of its universal functions, MOST apparent simplicity led to its widespread use in practically all numerical models of atmospheric flows. Focusing on stable and very stable conditions, this paper demonstrates how the functional form of MOST universal functions are intrinsically contained in the EFB closure theory; thus, once one adopts the EFB approach, MOST universal functions and all the possible relationships between them are fixed.

Theoretical framework

Energy and flux budget closure

Fluid mechanics equations allow to model the spatio-temporal evolution of a physical system such as the stable SL. Assuming the variables describing its state (the three wind speed components, the potential temperature, etc.) are stochastic and by applying the Reynolds decomposition to them, a SL model is capable of reconstructing the spatial and temporal evolution of the mean wind components (*U, V, W*), mean potential temperature (Θ), and relevant statistical moments - particularly the second-order ones, represented by the variance-covariance matrix of the Cartesian components of motion and the vector of turbulent heat fluxes[6,7,35]. The main issue in practically implementing such a fluid-dynamic model lies in its closure, i.e., in the fact that the description of turbulence is not closed and simplified or somehow semi-empirical relationships are needed to express higher-

order moments[15]. The following discussion will focus only on stable conditions and on the second order EFB closure.

The model examined by Zilitinkevich and colleagues[36–38] is a typical fluid dynamic model which includes a set of partial differential equations describing the mean fields of *U, V, W* and Θ. The stable SL is assumed to be hydrostatic (zero divergence), the Boussinesq approximation holds, and water vapor influence is indirectly accounted for by using the virtual potential temperature. Furthermore, in a hydrostatic model with horizontal dimensions larger than the vertical, subsidence W can be neglected, and the mean-field equations only contain three second-order moments to be determined, namely the Reynold stress components $\overline{u'w'}$ and $\overline{v'w'}$, along with the kinematic heat flux $\overline{w'\theta'}$[39]. The corresponding prognostic equations incorporate third-order moments and dissipation rates parametrizations.

Specifically, the third-order moments representing the vertical fluxes of $\overline{u'w'}$ and $\overline{v'w'}$ are parametrized as the composition of a term proportional to $\partial\overline{u_i'w'}/\partial z$ and a term of the form $E_z \cdot \partial U_i/\partial z$, where E_z is the vertical component of the turbulent kinetic energy (TKE) E_k, while the parametrization of the vertical flux of $\overline{w'\theta'}$ involves the sum of a term proportional to $\partial\overline{w'\theta'}/\partial z$. Following Kolmogorov[40,41], the dissipation rates are parameterized by assuming a proportional relationship between the moments themselves and a turbulent dissipation time scale, which is the same approach used in the Mellor-Yamada closure.

The TKE equation contains both $\partial U/\partial z$ and $\partial V/\partial z$, as well as a third-order term describing the flux of E_K and a dissipative term. The term related to shear-produced turbulence reflects the fact that E_K is primarily generated in the direction of the mean wind, i.e., directly feeding E_x which subsequently transfers energy to the other components E_y and E_z. Traditionally, the redistribution of energy among these different components is parametrized by the return-to-isotropy hypothesis[42], which assumes the transfer of turbulent energy from the richest to the poorest components. Since this hypothesis fails under very stable conditions, when turbulence tends to become two-dimensional, the EFB replace it with a novel mechanism to cope better with experimental evidences[36].

The closure also provides a prognostic equation for the turbulent potential energy (TPE) $E_p = 0.5 \cdot \beta \cdot \sigma_\theta^2 / (\partial\boldsymbol{\Theta}/\partial z)$, where $\beta = g/\boldsymbol{\Theta}_0$[43], which increases as TKE decreases due to the buoyancy sink. The equation contains both a third-order moment, assumed as proportional to $\partial \mathrm{E}_p/\partial z$, and a dissipation term proportional to TKE. The EFB closure is further extended by a prognostic relationship for the turbulent dissipation time scale and a set of diagnostic relations, derived from the steady-state version of the equations assuming horizontally homogeneous conditions, that describe the interplay between TKE components and the energy exchange between TKE and TPE. It is worth noting that EFB incorporates a set of numerical constants denoted as *C0*, *C1*, *C2*, *CF*, *CP*, *Cr* and *C*τ whose numerical values (0.125, 0.5, 0.72, 0.25, 0.86, 1.5 and 0.2, respectively), although tentatively determined through meteorological observations, laboratory experiments, DNS and large eddy simulations[38], still require definitive validation.

The closure is designed for a stable SL characterized by horizontal homogeneity and stationarity, which represents the paradigmatic scenario. As with MOST, the EFB closure has limitation when applied over heterogeneous terrain and in the presence of complex orography, where these assumptions are violated. Under paradigmatic conditions, the reference system is oriented such that the only non-zero mean component of the mean motion is *U*, directed along the x-axis, and the only non-zero component of the Reynolds stress is $\overline{u'w'}$[6,44–47]. As a result, all partial derivatives with respect to the x and y coordinates vanish, along with the total temporal derivative in the equations of the mean motion and the total temporal derivative in other equations. Finally, neglecting the divergence of third-order moments leads to the following set of diagnostic equations (see Kleeorin et al.[38] for further details and a rigorous derivation).

$$0 = -\tau\frac{\partial U}{\partial z} + \beta F_z - \frac{E_K}{t_T} \tag{1a}$$

$$0 = -F_z\frac{\partial \boldsymbol{\Theta}}{\partial z} - \frac{E_\theta}{C_p t_T} \tag{1b}$$

$$0 = -2E_z\frac{\partial \boldsymbol{\Theta}}{\partial z} + 2C_\theta\beta E_\theta - \frac{F_z}{C_F t_T} \tag{1c}$$

$$0 = -2E_z\frac{\partial U}{\partial z} - \frac{\tau}{C_\tau t_T} \tag{1d}$$

$$0 = \beta F_z + \frac{1}{2}Q_{zz} - \frac{E_K}{3t_T} \tag{1e}$$

where $\tau = \overline{u'w'}$, $F_z = \overline{w'\theta'}$, $E_\theta = 0.5\ \sigma_\theta^2$, t_T is the turbulence time scale and the inter-component energy exchange term Q_{zz} which is given by:

$$Q_{zz} = -\frac{2\,(1+C_r)}{3t_T}\,(3E_z - 3E_K + 2E_{int}) \tag{1f}$$

With

$$E_{int} = E_K + \frac{Ri_f}{R_\infty}\left(\frac{C_r}{1+C_r}\right)[C_0E_K - (1+C_0)\,E_z] \tag{1g}$$

where $R_\infty = 0.25$ is the flux Richardson number upper limit attainable in the steady-state regime of turbulence. Finally, the additional constant C_θ is defined as

$$C_\theta = \frac{C_r\,(1-2C_0)\cdot(1-R_\infty) - 3R_\infty}{[1+(C_p-1)\,R_\infty]\,[3+C_r\,(1-2C_0)]} \tag{1h}$$

The steady-state model considered above leads to universal relationships among Ri, Ri_f, the turbulent Prandtl Number Pr_T, the ratio of turbulent kinetic energy to turbulent potential energy (E_k/E_P), as well as the normalized vertical fluxes of momentum and heat. These relationships hold true as long as nonturbulent motions (internal gravity waves, Kelvin-Helmholtz shear instability, low-level jets, meso and sub-meso motions) are not considered, meaning that specific techniques[48,49] or more recent numerical approaches including machine learning applied to nonlinear systems[50], should be implemented to filter out nonturbulent contaminations when analysing experimental data to validate the model. In the following, we will refer to the steady-state EFB closure as the Zi2013 model[37].

Monin–Obukhov similarity theory and universal functions

Unlike EFB, MOST is based on dimensional analysis (Buckingham π theorem) applied to a SL in paradigmatic condition, where the turbulent state at height z is entirely determined by the buoyancy parameter $\mathbf{\beta}$, the mechanical forcing represented by the friction velocity $u_* = \sqrt{-\overline{u'w'}}$ and the thermal forcing described by the kinematic heat flux $\overline{w'\theta'}$, all combined in the single scaling parameter:

$$\zeta = \frac{z}{L} = -\frac{kzg}{\mathbf{\Theta}_r}\frac{\overline{w'\theta'}}{u_*^3} = \frac{kzg}{\mathbf{\Theta}_r}\frac{T_*}{u_*^2} \tag{2}$$

where $T_* = -\overline{w'\theta'}/u_*$ is the temperature scale and k the von Kármán constant. As a result, all the atmospheric parameters relevant to characterise the SL turbulence are expressed, when considered in their nondimensionalized form, as universal similarity functions of ζ[45]:

$$\frac{kz}{u_*}\frac{\partial U}{\partial z} = \mathbf{\Phi}_m(\zeta) \qquad \frac{kz}{T_*}\frac{\partial \mathbf{\Theta}}{\partial z} = \mathbf{\Phi}_h(\zeta) \tag{3a}$$

$$\frac{\sigma_u}{u_*} = \mathbf{\Phi}_{uu}(\zeta) \quad \frac{\sigma_v}{u_*} = \mathbf{\Phi}_{vv}(\zeta) \quad \frac{\sigma_w}{u_*} = \mathbf{\Phi}_{ww}(\zeta) \tag{3b}$$

$$\frac{\sigma_\theta}{|T_*|} = \mathbf{\Phi}_{\theta\theta}(\zeta) \tag{3c}$$

$$\frac{C_{V^2}\,z^{2/3}}{u_*^2} = \mathbf{\Phi}_{C_V^2}(\zeta) \quad \frac{C_{T^2}\,z^{2/3}}{T_*^2} = \mathbf{\Phi}_{C_T^2}(\zeta) \tag{3d}$$

$$\frac{kz\varepsilon_K}{u_*^3} = \mathbf{\Phi}_{\varepsilon_K}(\zeta) \quad \frac{kz\varepsilon_\theta}{u_* T_*^2} = \mathbf{\Phi}_{\varepsilon_\theta}(\zeta) \tag{3e}$$

where σ_u, σ_v, and are the wind components standard deviations, C_{V^2} and C_{T^2} the structure function parameters for velocity and temperature, and ε_K and ε_θ the dissipation rates for .E_k. and E_θ. Since $C_{V^2} = 4\alpha_1{\varepsilon_K}^{2/3} \cong 2.2{\varepsilon_K}^{2/3}$ and $C_{T^2} = 4\beta_1\varepsilon_\theta\varepsilon_K^{-1/3} \cong 3.2\varepsilon_\theta\varepsilon_K^{-1/3}$(where $\alpha_1 = 0.55$ and $\beta_1 = 0.8$ are Kolmogorov and Corrsin constants, respectively), equations (3d) can be expressed as

$$\frac{C_{V^2}z^{2/3}}{u_*^2} = \mathbf{\Phi}_{C_{V^2}}(\zeta) = 4\cdot\left(\mathbf{\Phi}_{\varepsilon_K}(\zeta)\right)^{2/3} \tag{3f}$$

$$\frac{C_{T^2}z^{2/3}}{T_*^2} = \mathbf{\Phi}_{C_{T^2}}(\zeta) = 3.2\cdot k^{-2/3}\cdot\mathbf{\Phi}_h(\zeta)\cdot\left(\mathbf{\Phi}_{\varepsilon_K}(\zeta)\right)^{-1/3} \tag{3g}$$

While MOST introduces several universal functions $\mathbf{\Phi}_x(\zeta)$, it does not define their exact analytical form. Furthermore, since MOST does not explicitly state the interdependence between variables as fluid-dynamic relationships do, it implicitly assumes that such interdependencies are intrinsic to the universal functions themselves that is, their mutual dependence arises not from separate empirical fitting, but from the underlying physical consistency of the system they represent.

MOST universal functions

In principle, $\Phi_x(\zeta)$ could be determined through curve fitting of experimental data, assuming they are not perturbated by nonturbulent motions or self-correlations, which are particularly critical in stable and very stable conditions[8–13]. In addition, MOST requires universal functions to be congruent with all the similarity relationships in which they are included; that is, they should not be determined independently of each other, disregarding any potential physical constraints or interrelations among them. While it is not feasible to establish a priori definitions of $\Phi_x(\zeta)$, dimensional analysis provides criteria for determining their asymptotic behaviours in both the adiabatic ($\zeta \to 0$) and the high stability ($\zeta \to \infty$) limit, when $\overline{w'\theta'}$ or z can be neglected).

The functional forms proposed in the exiting literature for the universal function under stable and very stable conditions frequently exhibit conflicting characteristics, potentially indicating that they may have been derived without taking adequate measures to avoid the adverse impact of nonturbulent motions and self-correlations. These two factors contribute to turbulent inflation and to the detection of spurious correlations, respectively.

Universal functions for wind and temperature gradients

Universal functions for wind and temperature gradients in equations (3a) have recently been discussed in Casasanta et al.[14], who reviewed the four main formulations proposed in the literature so far and assessed how they affect the theoretical behaviour of $\overline{w'\theta'}$ and T_* under stable and very stable conditions. None of them turned out to be completely consistent with the existing literature, while two of them produced highly unreliable expressions for both $\overline{w'\theta'}$ and T_*. The four formulations are summarised in Table 1, which also reports the values of the respective numerical constants obtained through curve fitting. Dimensional analysis suggests that both $\mathbf{\Phi}_m(\zeta)$ and $\mathbf{\Phi}_h(\zeta)$ tend towards a constant value as $\zeta \to 0$, and are linear when $\zeta \to \infty$. While the Businger-Dyer equations satisfy both these conditions, it is straightforward to verify that Beljaars-Holtslag's $\mathbf{\Phi}_h(\zeta)$, as well as CASES-99 and SHEBA formulations does not show the expected asymptotic behaviour when $\zeta \to \infty$.

Universal functions for the standard deviation of wind velocity

According to dimensional analysis, for the Universal Functions $\Phi_{uu}(\zeta)$, $\Phi_{vv}(\zeta)$, and $\Phi_{ww}(\zeta)$, the adiabatic limit should be a constant, just as the high stability limit should also be a constant. Naturally, these two asymptotic values can correspond to different numbers. Although data from a common 3D sonic anemometer could provide information for their characterization, the literature reports only a limited number of experimental campaigns with different data processing approaches in which all three universal functions were simultaneously determined under stable conditions. It is worth noting that the averaging time is crucial to filter out nonturbulent perturbations: excessively long averaging times can result in formulations that lack reliability. For instance, Mahrt et al.[25], (their Figure 2) observed a continuously increasing trend in $\Phi_{vv}(\zeta)$ with stability when using a 5-minute averaging time, which tended to a constant value when a shorter timeframe (100 s) was used. Analysing data from experimental campaigns carried out in rural and flat terrains, Andreas et al.[55] identified the relationship $\Phi_{\alpha\alpha}(\zeta) = a(1 + b\zeta)$(with $a = 2.55$ when $\alpha\alpha = uu,\ vv$ and $a = 1.20$ for $\alpha\alpha = ww$), which clearly does not tend towards a constant as $\zeta \to \infty$. A similar incontinency arise in the equation $\Phi_{\alpha\alpha}(\zeta) = a + b \cdot \zeta^c$ proposed by Pahlow et al.[56], where $a = 2.3,\ 2.0,\ 1.1$ and $b = 4.3,\ 4.0,\ 0.9$ for $\alpha\alpha = uu,\ vv,\ ww$, respectively, and c = 0.6 in all cases. The same issue occurs in the equation $\Phi_{\alpha\alpha}(\zeta) = a(1 + b\zeta)^{1/3}$ suggested in both Al-Jiboori et al.[57] and Quan and Hu[58], who used data acquired in urban and complex terrains In the latter two papers, the equation remains the same, but the values of the coefficients differ. Specifically, for $\alpha\alpha = uu,\ vv,\ ww$, the coefficients are $a = 1.76,\ 1.60,\ 1.22$ and $b = 2.39,\ 1.96, 1.05$ in the former, while in the latter they are $a = 1.96,\ 1.80,\ 1.42$ and $b = 2.07,\ 1.78,\ 0.54$. The difference between the various formulations becomes particularly evident at high stabilities, and it may be attributable to a range of factors, including the different averaging times used by various authors, variations in data processing techniques, the sensitivity of methods (whether linear or not) to outliers and the impact of self-correlation.

As a final remark, it is worth to highlight that existing literature supports the notion that $\Phi_{\varepsilon\theta}(\zeta)$—which indicates the universal function for the rate of temperature variance dissipation coincides with $\Phi_h(\zeta)$. Using Eq. (3g), it is straightforward to derive an expression for $\Phi_{C_T^2}(\zeta)$.

Universal function for the standard deviation of potential temperature

In this case as well, dimensional analysis suggests that the adiabatic limit for the universal function $\Phi_{\theta\theta}(\zeta)$, representing the standard deviation of potential temperature, is a constant. Similarly, its behaviour under high-stability conditions is also characterized by a constant—again, these two constants may not necessarily have identical values. When considering stable conditions exclusively, proposals for functional forms of $\Phi_{\theta\theta}(\zeta)$ are limited and show substantial discrepancies among them. Kaimal and Finnigan[45] proposed the equation $\mathbf{\Phi}_{\theta\theta}(\zeta) = 2.0 \cdot (1 + 0.5 \cdot \zeta)^{-1}$, Andreas et al.[55] recommended using a constant value $\Phi_{\theta\theta}(\zeta) = 3.2$, Pahlow et al.[56] presented the expressions $\Phi_{\theta\theta}(\zeta) = 2.0 \cdot (1 + 0.5 \cdot \zeta)^{-1}$, and Quan and Hu[58]

Formulation	$\mathbf{\Phi_m}(\boldsymbol{\zeta})$	$\mathbf{\Phi_h}(\boldsymbol{\zeta})$	References
Businger-Dyer	$1 + \beta_m\zeta$	$\alpha_h^{-1}(1 + \beta_h\zeta)$.	51
Beljaars–Holtslag	$1 + a\zeta + b\zeta \cdot [1 + c - d\zeta] \cdot\cdot exp(-d\zeta)$	$1 + a\boldsymbol{\zeta} \cdot \left[1 + \frac{2}{3}a\boldsymbol{\zeta}\right]^{1/2} + b\boldsymbol{\zeta}\cdot\cdot[1 + c - d\boldsymbol{\zeta}] \cdot \exp(-d\boldsymbol{\zeta})$	52
CASES-99	$1 + e\left(\frac{\zeta + \zeta^f\left(1+\zeta^f\right)^{\frac{1-f}{f}}}{\zeta + (1+\zeta^f)^{1/f}}\right)$	$1 + g\left(\frac{\zeta + \zeta^h\left(1+\zeta^h\right)^{\frac{1-h}{h}}}{\zeta + (1+\zeta^h)^{1/h}}\right)$	53
SHEBA	$1 + \frac{a_m\zeta}{(1+b_m\zeta)^{2/3}}$	$Pr_0\left(1 + \frac{a_h\zeta}{1+b_h\zeta}\right)$	54

Table 1. Universal functions for wind and temperature gradients as proposed in the literature, with $\beta_m = 5.3$, $\beta_h = 8.0$, $\alpha_h^{-1} = 0.95$, $a = 1.0$, $b = 0.67$, $c = 5.0$, $d = 0.35$, $e = 6.1$, $f = 2.5$, $g = 5.3$, $h = 1.1$, $a_m = a_h = 5$, $b_m = 0.3$, $b_h = 0.4$ and $Pr_0 = 0.98$.

formulated $\Phi_{\theta\theta}(\zeta) = 30.0 \cdot \zeta^{-1/3}$. As it is evident from Fig. 1, under very stable conditions the discrepancies between the expressions proposed by the various authors spans at least two orders of magnitude.

Universal function for the turbulent kinetic energy dissipation rate

Following dimensional analysis, $\Phi_{\varepsilon k}(\zeta)$ is expected to approach a constant value under adiabatic conditions, while it should increase linearly with ζ under high stability conditions. Existing literature generally supports the functional form $\Phi_{\varepsilon k}(\zeta) = a \cdot (1 + b \cdot \zeta)$, which shows the expected asymptotic behaviour. Variations emerge in the values attributed to the parameters a and b. Kaimal and Finnigan[45] propose $a = 1.0$ and $b = 5.0$, Högström[59] suggests $a = 1.24$ and $b = 3.8$, Pahlow et al.[56] report $a = 0.6$ and $b = 8.2$, while Hartogensis and De Bruin[60] find $a = 0.8$ and $b = 3.1$. In addition, considering $\Phi_{\varepsilon k}(\zeta)$ and using Eq. (3f), it is straightforward to derive the expression corresponding to the universal function $\Phi_{C_{V^2}}(\zeta)$.

Linking the EFB closure to MOST

Section "Linking the EFB closure to MOST" begins with a review of the steady-state Energy and Flux Budget (EFB) closure framework (Sect. 4.1–4.5) to establish the theoretical foundations, and concludes in Sect. 4.6 with the analytic derivation of all Monin-Obukhov similarity functions from the Zi2013 model.

The Zi2013 model[37] is the result of applying the prognostic relations introduced by Zi2013[37] to a stable, stationary, and horizontally homogeneous surface layer, with non-turbulent motions disregarded. Thus, refers to the very same physical environment as MOST. Section 4.1 to 4.5 provide a structured summary of the steady-state closure equations of Zi2013[37], with explicit references to the corresponding equation numbers from their original work to ensure traceability. These sections serve as a theoretical basis for the subsequent developments. The novel contribution of the present study begins in Sect. 4.6, where the functional forms of all the universal functions introduced in section "MOST universal functions" are analytically derived from the Zi2013 model[37]. This approach eliminates the need to infer these forms empirically from experimental data. In other words, as long as the Zi2013[37] model remains applicable, the functional forms of the MOST universal functions are inherently determined. While Zilitinkevich and colleagues use a somewhat unconventional definition of the stability parameter ζ, wherein the von Karman constant (k) is omitted, in the following discussion the more conventional definition of stability (Eq. 2, which incorporates k) is adopted.

Stability parameters

In addition to ζ, an alternative parameter that depends only on external forcings, rather than internal ones like T_* and u_* at the specific height considered, is the Gradient Richardson Number Ri, which is defined as follows:

$$Ri = \frac{g}{\Theta_r} \frac{\frac{\partial \bar{\Theta}}{\partial z}}{\left(\frac{\partial U}{\partial z}\right)^2} \tag{4a}$$

Unlike ζ, Ri depends exclusively on external forcings such as the gradients of the average potential temperature and of the mean wind speed, which are not directly measurable and has to be estimated based on two (or more) Θ and U measurements. While ζ is approximately proportional to the ratio between the height z and the characteristic length scale of the turbulent vortexes in the SL[61], Ri instead depends on the ratio between convective and mechanical forcings expressed as external variables that not directly associated with turbulence. Considering both point of views, it is possible to introduce a third stability parameter incorporating both external and internal forcings, the Flux Richardson Number Ri_f:

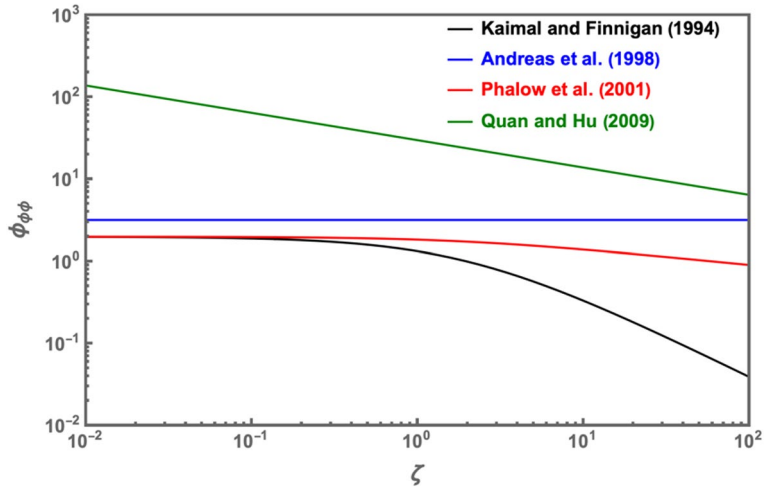

Fig. 1. Evolution of the four $\Phi_{\theta\theta}(\zeta)$ presented in section "Universal function for the standard deviation of potential temperature" as a function of the stability parameter ζ; discrepancies exceed two orders of magnitude at high stability.

$$Ri_f = \frac{g}{\Theta_r} \frac{\overline{w'\theta'}}{\overline{u'w'}\frac{\partial U}{\partial z}} \tag{4b}$$

In this case, stability is characterised in terms of energy, since under stable paradigmatic conditions Ri_f is linked to the turbulent kinetic energy balance[31]. Differently from Ri, Ri_f is expected to reach an asymptotic value between 0.2 and 0.25 for $\zeta \to \infty$, as confirmed by a number of both experimental and modelling studies[17,18,30,62–65]. Following this approach, more recently Zilitinkevich et al.[66] proposed the Energy Richardson Number Ri_E, which is defined as the ratio between turbulent potential and kinetic energy:

$$Ri_E = \frac{E_P}{E_K} = \frac{\beta^2}{\frac{\partial \theta}{\partial z}} \frac{\sigma_\theta^2}{(\sigma_u^2 + \sigma_v^2 + \sigma_w^2)} \tag{4c}$$

From the previous equation it is clear that Ri_E cannot be defined under strictly neutral conditions, where $\partial\Theta/\partial z \to 0$, while it is expected to approach an asymptotic value of 0.155 under highly stable conditions[66]. In addition, Ri_E is particularly valuable within the EFB framework, as in this particular closure turbulence is sustained by velocity shear regardless of stratification, and any alteration in E_K is compensated by a corresponding adjustment in E_P to ensure the conservation of total energy.

Flux Richardson number and MOST universal functions for wind gradients

The functional form of the universal function for wind gradients is provided in Zi2013, and it is presented here for the sake of completeness. Considering the existence of an asymptotic value (R_∞) for Ri_f and the E_K budget under paradigmatic condition, the product $kz/u_* \ \partial U/\partial z$ converges to 1 under neutrally stratified conditions, essentially recovering the well-known wall law. Conversely, in highly stable conditions this product is expected to vary linearly as R_∞^{-1}. A straightforward interpolation between these two results leads to the following expression, which is formally identical to MOST Eq. (3a):

$$\frac{\partial U}{\partial z} = \frac{u_*}{kz} \cdot \left(1 + R_\infty^{-1}\zeta\right) \tag{5}$$

Where

$$1 + R_\infty^{-1}\zeta = \Phi_m(\zeta) \tag{6}$$

Even though an interpolation is not the only possible choice, it leads to a familiar result. Assuming $R_\infty = 0.2$ [66] (their Figure 4) and $R_\infty^{-1} = 5$ the previous equation coincides with the Businger-Dyer formulation reported in Table 1. The Businger-Dyer equation, initially derived from curve fitting under weak to moderate stability conditions, is now extended to encompass all stable conditions and is directly linked to Zi2013 closure[37]. Also, this result highlights the crucial role of the asymptotic value for Ri_f, which, as demonstrated in the next subsections, acts as a fundamental constant.

As shown in Zi2013[37], combining Eq. (5) with (4b) yields to the following universal function for Ri_f

$$Ri_f \equiv_{Ri_f}(\zeta) = \frac{\zeta}{1 + R_\infty^{-1}\zeta} = \frac{\zeta}{\Phi_m(\zeta)} \tag{7}$$

which is fully consistent with MOST (see, e.g[14]., Eq. 6) but specifies a fixed analytical form for $\Phi_m(\zeta)$. Figure 2 illustrates the Ri_f behaviour as a function of ζ for the four different $\Phi_m(\zeta)$ formulations provided in Table 1. As anticipated, only the Businger-Dyer expression successfully replicates the expected Ri_f behaviour, in contrast to the other three formulations, which either diverge or converge to a value higher than expected.

Gradient Richardson number and MOST universal functions for temperature gradients

As for the other MOST universal functions, linear relation the universal function for the Gradient Richardson Number is described in Zi2013[37] (their Eq. 82), which incorporates a number of constants, including R_∞^{-1}:

$$\begin{aligned} Ri \ \ &\equiv_{Ri}(\zeta) = \frac{C_\tau \zeta}{C_F\left(1 + R_\infty^{-1}\zeta\right)}\left[1 + \frac{\alpha_1\zeta + \alpha_2\zeta^2}{1 + x\zeta}\right] \quad C_\tau = 0.20, \\ C_F \ \ &= 0.25, \ \alpha_1 = 0.18, \ \alpha_2 = 0.16, \ \alpha_2 = 1.42 \end{aligned} \tag{8}$$

where the parameters α_1, α_2 and α_3 are defined by Zi2013 Eq. 83 to 85[37]. According to the previous equation, Ri increases monotonically with ζ without reaching any asymptotic value; thus, it depends solely on the mean flow state and its growth is unrestricted by internal turbulence.

On the other hand, combining MOST Equations (3a) and (4a) with (8) and solving for $\Phi_h(\zeta)$ yields the expression:

$$\Phi_h(\zeta) =_{Ri}(\zeta) \frac{(\Phi_m(\zeta))^2}{\zeta} = \zeta \frac{Ri(\zeta)}{\frac{2}{Ri_f}(\zeta)} \tag{9}$$

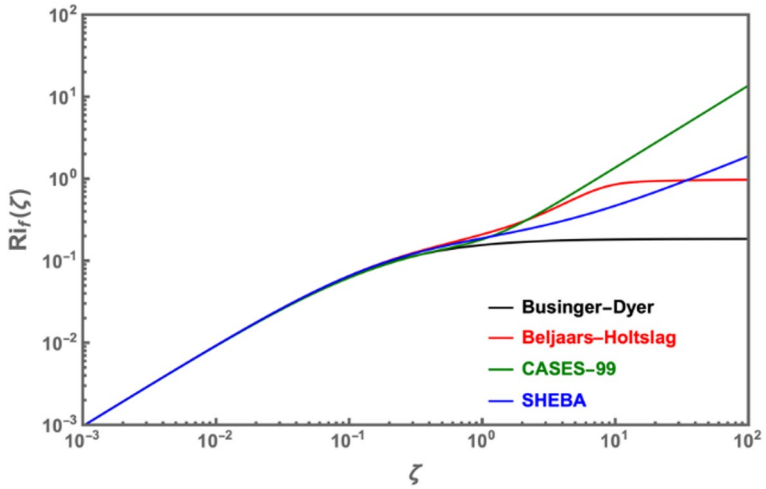

Fig. 2. Evolution of Ri_f as a function of ζ for the four $\Phi_m(\zeta)$ formulations reported in Table 1; only the Businger–Dyer formulation converges to the expected value.

Substituting Eq. (8) into (9) allows to retrieve a formulation for $\Phi_h(\zeta)$ whose analytical form is already determined and has not to be inferred from experimental data:

$$\Phi_h(\zeta) = \frac{C_\tau}{C_F}\left(1 + R_\infty^{-1}\zeta\right)\left[1 + \frac{\alpha_1\zeta + \alpha_2\zeta^2}{1 + \alpha_3\zeta}\right] \tag{10}$$

It is worth emphasizing that while $\Phi_h(\zeta)$ follows a linear dependence on ζ, the formulation for $\Phi_h(\zeta)$ derived from it depends on ζ quadratically. From a practical point of view, to avoid any possible self-correlation it is recommended to determine all the variables in the following order: R_∞, Φ_m, $\Im_{Ri}$ and finally Φ_h typically, universal functions are obtained independently of each other, neglecting any possible relation between them, but Eq. (9) clearly shows that $\mathbf{\Phi}_h(\zeta)$ and $\mathbf{\Phi}_m(\zeta)$ are interconnected. The resulting formulations are valid at any level of stability and fully congruent with each other. They also account for the existence of a minimum in $\overline{w'\theta'}$ and T_*[14], as well as for a finite asymptotic value for Ri_f and an unlimited but linear growth of Ri with ζ.

In addition, Zi2013[37] also retrieve the following formulation for the Prandtl turbulent Number:

$$Pr_T(\zeta) = \frac{C_\tau}{C_F}\cdot\left[1 + \frac{\alpha_1\zeta + \alpha_2\zeta^2}{1 + \alpha_3\zeta}\right] \tag{11}$$

When neutrality is approached as defined in Zi2013 (Eq. 57)[37], $Pr_T(0) = C_\tau/C_F = 0.8$. This value is lower than typically estimated from experimental data (e.g[67]), which is close to 0.95. At high stability, instead, $Pr_T(\zeta)$ increases linearly with ζ.

Universal functions for the inter-component exchange of turbulent kinetic energy

As discussed in Zi2013, the stable SL is characterised by a continuous exchange of TKE among different components, which clearly conflict with the assumption of Rotta's return to isotropy[42]. Furthermore, while this energy exchange occurs between TKE vertical and horizontal components, there is an additional exchange of energy between E_k and E_P[18,38].

The Zi2013 model[37] allows for the determination of the shares between different components of turbulent kinetic energy, namely, $A_x = E_x/E_K$, $A_y = E_y/E_K$, $A_z = E_z/E_K$, and describes their behaviour as a function of the stability parameter ζ(Zi2013 Eq. 50 subsequent[36]). When $\zeta \to 0$ and neutrality is approached, the longitudinal component of E_K is greater than the transverse one, which in turn is greater than the vertical component ($A_x = 0.5 > A_y = 0.3 > A_z = 0.2$). Conversely, as stability increases and $\zeta \to \infty$, most of the turbulent kinetic energy is distributed equally between the two horizontal components ($A_x \cong A_y = 0.49$), while the vertical component decreases significantly but does not vanish ($A_z = 0.03$), in agreement with Zi2023 (Eq. 80).

The universal function obtained in Zi2013[37] for A_z as a function of ζ is expressed by the following equation:

$$A_z(\zeta) = \frac{R_\infty C_r + \zeta\cdot\left[C_r(1 - 2C_0) - \frac{3R_\infty(R_\infty+\zeta)}{R_\infty+(1-R_\infty)\cdot\zeta}\right]}{3R_\infty(1 + C_r) + \zeta\cdot[3 + C_r(1 - 2C_0)]} \tag{12a}$$

In the previous equation, once again, the persistence of turbulence even under extreme stability is signified by the parameter R_∞, while $C_r = 1.5$ and $C_0 = 1.25$ are associated with the parametrization of E_K exchanges

between different components, contradicting Rotta's return to isotropy hypothesis. Under adiabatic conditions, $A_z(\zeta)$ reaches a constant value determined by C_r,

$$A_z(0) = \frac{C_r}{3\cdot(1+C_r)}, \tag{12b}$$

while its asymptotic value is given by the following relationship:

$$A_z(\infty) = \frac{C_r(1-2C_0) - 3\left(R_\infty^{-1}-1\right)^{-1}}{3 + C_r(1-2C_0)} \tag{12c}$$

In addition, the universal functions for longitudinal and transverse shares, which depend on Ri_f although the dependence on ζ can always be determined using Eq. (7) are as follows (see Zi2013, Eq. 50a–50c):

$$A_x(Ri_f) = \frac{1}{(1+C_r)(1-Ri_f(\zeta))} + \left(1 - C_1 - C_2\frac{Ri_f(\zeta)}{R_\infty}\right)\cdot A_z(0)\cdot \left[1 + \frac{Ri_f(\zeta)}{R_\infty}\left[C_o - (1+C_0)\cdot A_z(\zeta)\right]\right] \tag{13}$$

$$A_y(Ri_f) = \left(1 + C_1 + C_2\frac{Ri_f}{R_\infty}\right)\cdot A_z(0)\cdot\left[1 + \frac{Ri_f}{R_\infty}\left[C_o - (1+C_0)\cdot A_z(\zeta)\right]\right] \tag{14}$$

Nevertheless, it is worth noticing that the three components A_x, A_y and A_z cannot be considered as independent of each other, as they have to satisfy the obvious constrain $A_x + A_y + A_z = 1$.

Universal functions for normalized vertical fluxes

Under paradigmatic conditions, turbulence within the SL is driven only by vertical fluxes of momentum and sensible heat. For the vertical flux of momentum, the[37] model provides a relationship expressed as a function of both Ri_f and ζ:

$$\left(\frac{\tau}{E_K}\right)^2 = \frac{2C_\tau\cdot A_z(\zeta)}{(1-Ri_f(\zeta))} = 2C_\tau\cdot A_z(\zeta)\cdot\frac{1+R_\infty^{-1}\zeta}{1+\left(R_\infty^{-1}-1\right)\cdot\zeta} \equiv {}_\tau(\zeta) \tag{15}$$

where $\tau = u_*^2$. Given the known behaviour of Ri_f as a function of ζ and the expression for $A_z(\zeta)$ from Eq. (12a), the previous relation defines ${}_\tau$ as a universal function of ζ, with its analytical form fully determined. For typical values of the constants C_τ, C_r, C_0 and R_∞, the normalised vertical flux ranges between 0.08 (at $\zeta = 0$) and 0.016 (for $\zeta \to \infty$).

From Eq. (15), it is straightforward to derive the normalized fluxes with respect to E_x, E_y and E_z:

$$\frac{\tau}{E_x} = \frac{(\Im_\tau(\zeta))^{1/2}}{A_x(\zeta)} = \sqrt{2C_\tau}\cdot\frac{(A_z(\zeta))^{1/2}}{A_x(\zeta)}\cdot\left(\frac{1+R_\infty^{-1}\zeta}{1+\left(R_\infty^{-1}-1\right)\cdot\zeta}\right)^{1/2} \equiv \Im_{\tau x}(\zeta) \tag{15a}$$

$$\frac{\tau}{E_y} = \frac{(\Im_\tau(\zeta))^{1/2}}{A_y(\zeta)} = \sqrt{2C_\tau}\cdot\frac{(A_z(\zeta))^{1/2}}{A_y(\zeta)}\cdot\left(\frac{1+R_\infty^{-1}\zeta}{1+\left(R_\infty^{-1}-1\right)\cdot\zeta}\right)^{1/2} \equiv \Im_{\tau y}(\zeta) \tag{15b}$$

$$\frac{\tau}{E_z} = \frac{(\Im_\tau(\zeta))^{1/2}}{A_z(\zeta)} = \sqrt{2C_\tau}\cdot(A_z(\zeta))^{-1/2}\cdot\left(\frac{1+R_\infty^{-1}\zeta}{1+\left(R_\infty^{-1}-1\right)\cdot\zeta}\right)^{1/2} \equiv \Im_{\tau z}(\zeta) \tag{15c}$$

The behaviour of the three normalized fluxes as a function of ζ is illustrated in Fig. 3 (left panel). With increasing stability, both $\Im_{\tau x}(\zeta)$ and $\Im_{\tau y}(\zeta)$ decrease towards the asymptotic value of 0.26, while ${}_{\tau z}(\zeta)$ increases up to 4.20, reflecting the distribution of kinetic energy discussed in the previous subsection.

Similarly, Zi2013[37] determines an expression for the dimensionless turbulent flux of potential temperature,

$$\frac{\overline{w'\theta'}^2}{E_K E_\theta} = \frac{2C_\tau}{C_p}\cdot\frac{A_z(\zeta)}{Pr_T(\zeta)}, \tag{16a}$$

which can be readily rearranged to derive the normalized vertical flux of potential temperature expressed as a universal function of ζ:

$$\frac{\overline{w'\theta'}^2}{E_z E_\theta} = \frac{2C_\tau}{C_p\cdot Pr_T(\zeta)} \equiv {}_{w\theta}(\zeta) \tag{16b}$$

The behaviour of ${}_{w\theta}(\zeta)$ is shown in Fig. 3 (right panel). At neutrality, ${}_{w\theta}(0) = 2C_\tau/(C_p Pr_T(0)) = 0.58$, while it decreases linearly as ζ increases under highly stable conditions.

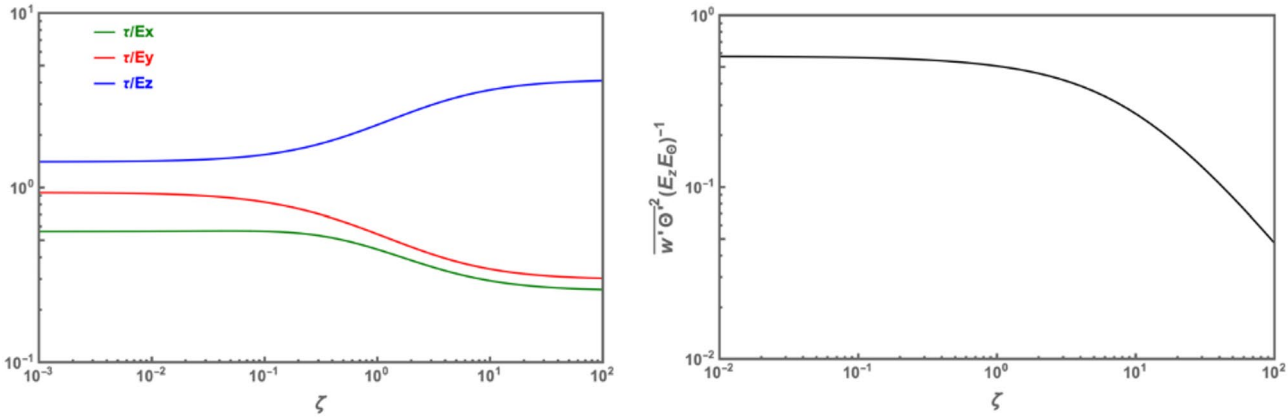

Fig. 3. Behaviour of the three normalized vertical fluxes of momentum (left panel) and potential temperature (right panel) as a function of ζ; the contrasting trend of τ/E_z compared to both τ/E_x and τ/E_y reflects the TKE exchange among components.

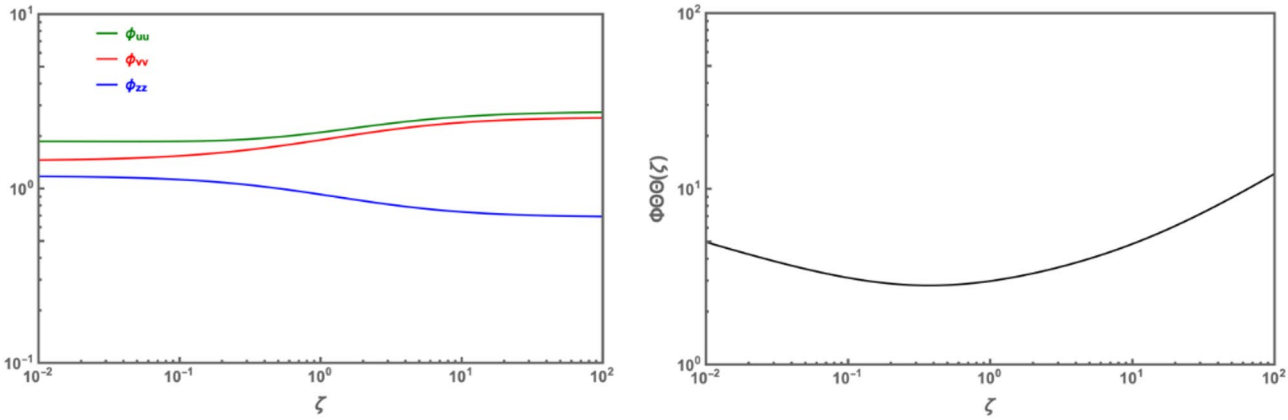

Fig. 4. Behaviour of the universal functions for standard deviations (left panel) and potential temperature (right panel) as a function of ζ; according to the intercomponent exchange of TKE, wind standard deviations tend towards horizontal isotropy as stability increases.

Universal functions for standard deviations of potential temperature and wind components

Universal functions for the standard deviations of both potential temperature (σ_θ) and wind components ($\sigma_u,\ \sigma_v,\ \sigma_w$) can be derived from normalised vertical fluxes. Recalling MOST Eq. (3b) and inverting Equations (15), where $\tau = u_*^2$ and $E_\propto = 0.5\ \sigma_\propto^2 (\propto = u, v, w)$, yields

$$\Phi_{uu}(\zeta) = \frac{\sigma_u}{u_*} = \sqrt{\frac{2}{\Im_{\tau x}(\zeta)}} = \sqrt{2A_x(\zeta)} \left[\frac{1 + \left(R_\infty^{-1} - 1\right)\cdot\zeta}{2C_\tau \cdot A_z(\zeta)\cdot\left(1 + R_\infty^{-1}\zeta\right)}\right]^{1/4} \tag{17a}$$

$$\Phi_{vv}(\zeta) = \frac{\sigma_v}{u_*} = \sqrt{\frac{2}{\Im_{\tau y}(\zeta)}} = \sqrt{2A_y(\zeta)} \left[\frac{1 + \left(R_\infty^{-1} - 1\right)\cdot\zeta}{2C_\tau \cdot A_z(\zeta)\cdot\left(1 + R_\infty^{-1}\zeta\right)}\right]^{1/4} \tag{17b}$$

$$\Phi_{ww}(\zeta) = \frac{\sigma_w}{u_*} = \sqrt{\frac{2}{\Im_{\tau z}(\zeta)}} = \sqrt{2} \left[\frac{A_z(\zeta)}{2C_\tau}\cdot\frac{1 + \left(R_\infty^{-1} - 1\right)\cdot\zeta}{1 + R_\infty^{-1}\zeta}\right]^{1/4} \tag{17c}$$

These equations provide expressions for the standard deviations of wind components normalised by u_*, in terms of ζ and the universal functions $A_x(\zeta)$, $A_y(\zeta)$ and $A_z(\zeta)$. Their behaviour as a function of stability is represented in Fig. 4 (left panel). According to the inter-component exchange of TKE described in Sect. 4.4, as stability increases, both $\Phi_{uu}(\zeta)$ and $\Phi_{vv}(\zeta)$ reach asymptotic values close to each other (2.90 and 2.62, respectively), tending towards horizontal isotropy, while $\Phi_{ww}(\zeta)$ decreases. Under adiabatic conditions

($\zeta = 0$), the vertical component depends solely on the two constants C_τ and C_r, while in the expressions for the horizontal components, C_1 is also included:

$$\left(\frac{\sigma_w}{u_*}\right)_0 = \left(\frac{2A_z^0}{C_\tau}\right)^{1/4} = \left(\frac{2}{3}\cdot\frac{C_r}{C_\tau\left(1+C_r\right)}\right)^{1/4} \tag{18a}$$

$$\left(\frac{\sigma_v}{u_*}\right)_0 = \left(1+C_1\right)^{1/2}\cdot\left(\frac{\sigma_w}{u_*}\right)_0 \tag{18b}$$

$$\left(\frac{\sigma_u}{u_*}\right)_0 = \left(\frac{3}{C_r}+1-C_1\right)^{1/2}\left(\frac{\sigma_w}{u_*}\right)_0 \tag{18c}$$

In addition, Eqs. (17a–17c) are linked together by Eq. (15), which serves as a constrain:

$$\Phi_{uu}^2\left(\zeta\right)+\Phi_{vv}^2\left(\zeta\right)+\Phi_{ww}^2\left(\zeta\right) = 2\cdot\Im_\tau^{-1/2}\left(\zeta\right) \tag{18d}$$

Similarly, the universal function for the standard deviation of potential temperature can be obtained by substituting the expressions for E_K and E_θ into Eq. (16b), and using Eq. (17c):

$$\frac{\sigma_\theta}{T_*} = \sqrt{2\,\frac{\Im_{\tau z}\left(\zeta\right)}{\Im_{w\theta}\left(\zeta\right)}} \tag{19a}$$

Recalling MOST Eq. (3c), the previous expression directly yields:

$$\Phi_{\theta\theta}\left(\zeta\right) = \frac{\sigma_\theta}{T_*} = \frac{\sqrt{2C_pPr_T\left(\zeta\right)}}{\left(2C_\tau A_z\left(\zeta\right)\right)^{\frac{1}{4}}}\left(\frac{1+R_\infty^{-1}\zeta}{\left[1+\left(R_\infty^{-1}-1\right)\right]\zeta}\right)^{\frac{1}{4}} \tag{19b}$$

As shown in the right panel of Fig. 4, $\Phi_{\theta\theta}$ gradually increases with stability, and only when $\zeta > 1$ its growth becomes significant. Also in this case, $\Phi_{\theta\theta}\left(\zeta\right)$ cannot be considered independent from the other universal function, as it is linked to $\Phi_{ww}\left(\zeta\right)$ though the following constrain relationship:

$$\Phi_{ww}\left(\zeta\right)\cdot\Phi_{\theta\theta}\left(\zeta\right) = 2\Im_{w\theta}^{-1/2}\left(\zeta\right) \tag{20}$$

Relationships between the energy Richardson number and universal functions

The ratio between the turbulent potential and kinetic energy, $Ri_E = \frac{E_p}{E_K}$, plays a crucial role in the EFB closure, and it can be expressed as a function of just the stability level:

$$Ri_E = \frac{E_p}{E_K} = C_p\frac{\zeta}{1+\left(R_\infty^{-1}-1\right)\zeta} \equiv_{Ri_E}\left(\zeta\right) \tag{21a}$$

Here, the numerical constant C_p expressed the difference between E_p and E_K dissipation rates, while R_∞ remains once again a key parameter. Similarly to Ri_f, Ri_E reaches an asymptotic value between 0.14 and 0.15 for $\zeta \to \infty$[66]:

$$Ri_{E_\infty} = \frac{C_p}{R_\infty^{-1}-1} \tag{21b}$$

When considering only the vertical component of TKE, Eq. (21a) becomes:

$$Ri_{Ez}\left(\zeta\right) = \frac{E_p}{E_z} = \frac{Ri_E\left(\zeta\right)}{A_z\left(\zeta\right)} \equiv_{Ri_{Ez}}\left(\zeta\right) \tag{22a}$$

Replacing the definitions of both E_p and E_z in the previous expression, and using MOST Eqs. (3a), (3b) and (3c), leads to:

$$\Im_{Ri_{Ez}}\left(\zeta\right) = \zeta\frac{\Phi_{\theta\theta}^2\left(\zeta\right)}{\Phi_h\left(\zeta\right)\cdot\Phi_{ww}^2\left(\zeta\right)} \tag{22b}$$

The previous relationship represents an additional constrain, establishing a link between $_{Ri_{Ez}}\left(\zeta\right)$and the stability parameter ζ, as well as three other MOST universal functions whose functional forms are defined by Eqs. (19a), (20) and (10).

Similarly, when examining the horizontal components of TKE, Eq. (21a) gives:

$$Ri_{Ex}\left(\zeta\right) = \frac{Ri_E\left(\zeta\right)}{A_x\left(\zeta\right)} \equiv \Im_{Ri_{Ex}}\left(\zeta\right) \tag{23a}$$

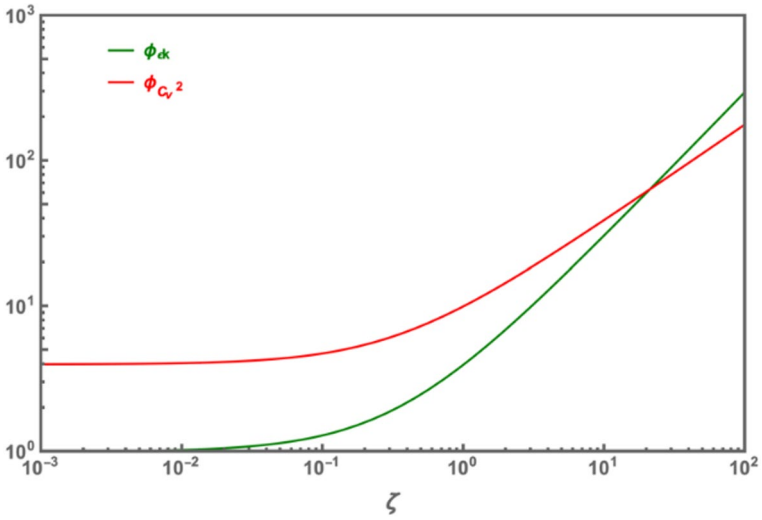

Fig. 5. Evolution of Φ_{ε_K} and $\Phi_{C_{V^2}}$ as a function of ζ; linear and two-thirds-power scalings support the functional forms proposed in previous literature.

$$Ri_{Ey}(\zeta) = \frac{Ri_E(\zeta)}{A_y(\zeta)} \equiv \Im_{Ri_{Ey}}(\zeta) \tag{23b}$$

As a result, the mechanism of energy exchange among the three TKE components, as well as between the potential and kinetic turbulent energy, modulated by the vertical mean gradient of potential temperature within MOST framework, is reflected here in Eqs. (21a) and (23a, 23b).

For the sake of completeness, it is worth mentioning here that the total turbulent energy, E, is defined by the standard deviations of potential temperature and wind components, as well as the vertical gradient of the mean temperature:

$$E = \frac{1}{2}\left[\left(\sigma_u^2 + \sigma_u^2 + \sigma_u^2\right) + \beta^2 \frac{\sigma_\theta^2}{\partial\Theta/\partial z}\right] \tag{24}$$

Following Zi2013, the ratio between E_p and E is also a universal function of ζ:

$$\frac{E_p}{E} = \frac{C_p R_\infty \zeta}{R_\infty + [1 + R_\infty (C_p - 1)] \cdot \zeta} \equiv \Im_E(\zeta) \tag{25}$$

Universal functions for dissipation rates and structure parameters

According to Zilitinkevich at al.[66], the ratio between the dissipation rate for $E_K(\varepsilon_K)$ and the friction velocity, is expressed by the following nondimensional relationship:

$$\frac{kz\varepsilon_K}{u_*^3} = \frac{1 - Ri_f}{1 - \frac{Ri_f}{R_\infty}} = \left[1 + \left(R_\infty^{-1} - 1\right) \cdot \zeta\right] \tag{26}$$

Straightforward comparison between the previous equation and MOST Eq. (3e) yields:

$$\Phi_{\varepsilon_k}(\zeta) = \left[1 + \left(R_\infty^{-1} - 1\right) \cdot \zeta\right] \tag{26a}$$

which is a linear function of the stability parameter ζ.

Furthermore, using MOST Eq. (3f) with the previous, the universal function for C_{V^2} is expressed as:

$$\Phi_{C_{V^2}}(\zeta) = 4 \cdot \left(1 + \left(R_\infty^{-1} - 1\right) \cdot \zeta\right)^{2/3} \tag{27}$$

The behaviour of both $\mathbf{\Phi}_{\varepsilon_K}(\zeta)$ and $\mathbf{\Phi}_{C_{V^2}}(\zeta)$ as a function of ζ is illustrated in Fig. 5.

In addition, using Eq. (7), these two universal functions can also be expressed as a function of $\Im_{Ri_f}(\zeta)$:

$$\Phi_{\varepsilon_K}(\zeta) = \left(1 - \Im_{Ri_f}(\zeta)\right) \cdot \frac{\zeta}{\Im_{Ri_f}(\zeta)} \tag{28a}$$

$$\Phi_{C_{V^2}}(\zeta) = 4 \cdot \left[\left(1 - \Im_{Ri_f}(\zeta)\right) \cdot \frac{\zeta}{\Im_{Ri_f}(\zeta)} \right]^{2/3} \tag{28b}$$

Regarding the universal function for $\Phi_{\varepsilon_\theta}(\zeta)$, its functional form coincides with $\Phi_h(\zeta)$ and does not need to be determined separately, as demonstrated in Kaimal and Finnigan[45]. Such a result is the direct consequence of assuming a paradigmatic SL, where most of the temperature standard deviation produced is destroyed by molecular dissipation. Also in this case, the universal function for C_T^2 can be readily obtained from MOST Eq. (3 g), while both $\Phi_{\varepsilon\theta}(\zeta)$ and $\Phi_{C_{T^2}}(\zeta)$ can be expressed as a function of $\Im_{Ri}(\zeta)$ though Eq. (7):

$$\Phi_{\varepsilon_\theta}(\zeta) = \zeta \cdot \Im_{Ri}(\zeta) \cdot \left(\Im_{Ri_f}(\zeta)\right)^{-2} \tag{29a}$$

$$\Phi_{C_{T^2}}(\zeta) = 3.2k^{-2/3} \cdot \frac{\Im_{Ri}(\zeta)}{{\Im_{Ri_f}}^2(\zeta)} \cdot \left(\frac{\zeta^2 \Im_{Ri_f}(\zeta)}{1 - \Im_{Ri_f}(\zeta)} \right)^{1/3} \tag{29b}$$

Discussion

As discussed in Sect. 3, MOST similarity relationships (3) describe the behaviour of the main SL parameters as a function only of the stability parameter ζ. These relationships are derived through dimensional analysis and depend on ten universal functions, namely Φ_m, Φ_h, Φ_{uu}, Φ_{vv}, Φ_{ww}, $\Phi_{\theta\theta}$, $\Phi_{C_{V^2}}$, $\Phi_{C_{T^2}}$, Φ_{ε_K}, $\Phi_{\varepsilon_\theta}$, whose functional forms are not intrinsically determined and must be experimentally inferred, typically through curve fitting. So far, this approach has presented several issues. First, often experimental campaigns do not explicitly consider non-turbulent motions, that can significantly influence turbulence measurements. Second, the formulations obtained through curve fitting typically do not account for self-correlation, which may result spurious correlations (see, e.g[12]). Third, these formulations are generally obtained independently of one another, neglecting potential physical constrain relationship among them. As a results, a set of generally accepted formulations has yet to be established. This is especially evident under stable and very stable conditions, where existing formulations proposed in literature often fail to align with both theoretical and experimental results. For instance, as discussed in Casasanta et al.[14] the four main formulations suggested to date[51,52,54,68] are not capable of reproducing the theoretical behaviour of the kinematic heat flux and the temperature scale.

On the other hand, the EFB closure involves a total of 15 universal functions $\Im_{Ri_f}(\zeta)$, $\Im_{Ri}(\zeta)$, $A_x(\zeta)$, $A_y(\zeta)$, $A_z(\zeta)$, $\Im_\tau(\zeta)$, $\Im_{w\theta}(\zeta)$, $\Im_{\tau x}(\zeta)$, $\Im_{\tau y}(\zeta)$, $\Im_{\tau z}(\zeta)$, $Pr_T(\zeta)$, $\Im_{Ri_{Ex}}(\zeta)$, $\Im_{Ri_{Ey}}(\zeta)$, $\Im_{Ri_{Ez}}(\zeta)$ and $\Im_E(\zeta)$ each defined by a predetermined analytical form, with only numerical coefficients left to be determined. While a definitive validation of their values is still required, it is worth noting that all the constants have already been estimated through both experimental and modelling studies and are generally considered reasonably reliable[38]. As detailed in section "Linking the EFB closure to MOST", since the physical SL under consideration remains unchanged, the MOST universal functions can be expressed in terms of the EFB closure functions, thus uniquely identifying their analytical forms.

Focusing on stable and very stable conditions, we demonstrated how the functional forms of MOST universal functions are intrinsically contained in the EFB closure theory; thus, once one adopts the EFB approach, MOST universal functions and all the possible relationships between them are fixed. A summary of the ten MOST functions expressed as a function of one or more EFB functions is reported below.

$$\Phi_m(\zeta) = \frac{\zeta}{\Im_{Ri_f}(\zeta)} \tag{7}$$

$$\Phi_h(\zeta) = \zeta \frac{\Im_{Ri}(\zeta)}{\Im^2_{Ri_f}(\zeta)} \tag{9}$$

$$\Phi_{uu}(\zeta) = \sqrt{\frac{2}{\Im_{\tau x}(\zeta)}} \tag{17a}$$

$$\Phi_{vv}(\zeta) = \sqrt{\frac{2}{\Im_{\tau y}(\zeta)}} \tag{17b}$$

$$\Phi_{ww}(\zeta) = \sqrt{\frac{2}{\Im_{\tau z}(\zeta)}} \tag{17c}$$

$$\Phi_{\theta\theta}(\zeta) = \sqrt{2\,\frac{\Im_{\tau z}(\zeta)}{\Im_{w\theta}(\zeta)}} \tag{19a}$$

$$\Phi_{\varepsilon_K}(\zeta) = \left(1 - \Im_{Ri_f}(\zeta)\right) \cdot \frac{\zeta}{\Im_{Ri_f}(\zeta)} \tag{28a}$$

$$\Phi_{C_{V^2}}(\zeta) = 4 \cdot \left[\left(1 - \Im_{Ri_f}(\zeta)\right) \cdot \frac{\zeta}{\Im_{Ri_f}(\zeta)} \right]^{2/3} \tag{28b}$$

$$\Phi_{\varepsilon_\theta}(\zeta) = \zeta \cdot \Im_{Ri}(\zeta) \cdot \left(\Im_{Ri_f}(\zeta)\right)^{-2} \tag{29a}$$

$$\mathbf{\Phi}_{C_{T^2}}(\zeta) = 3.2\mathrm{k}^{-2/3} \cdot \frac{\Im_{\mathrm{Ri}}(\zeta)}{\Im_{\mathrm{Ri_f}}{}^2(\zeta)} \cdot \left(\frac{\zeta^2 \Im_{\mathrm{Ri_f}}(\zeta)}{1 - \Im_{\mathrm{Ri_f}}(\zeta)}\right)^{1/3} \tag{29b}$$

In addition, the connection between MOST and EFB closure functions allowed to establish the three new constrain relationships (18d), (20) and (22b), which link MOST universal functions to one another. More generally, as previously stated in literature (e.g[14]), the existence of these relationships indicates that the universal functions cannot be considered independently, thus reflecting the fact that MOST requires universal functions to be congruent with all the similarity relationship in which they are included. This interdependence among universal functions is consistent with Dias[69], which demonstrates that the nondimensionalization of the fluid-dynamic equations for second-order moments, under the assumption of stationarity, surface uniformity and homogeneity, leads to a new set of algebraic equations depending solely on the stability parameter ζ and the MOST universal functions. To the best of our knowledge, Dias[69] remains the only study explicitly addressing this topic.

The proposed functional forms were derived analytically and still require validation[38], either through a specifically designed field campaign or a thorough analysis of datasets already available in the literature, see e.g., Mauritsen T, Svensson G[18], which includes observations of stably stratified turbulence from six different studies. From an experimental perspective, a campaign aiming at validating these universal functions should meet a number of requirements, starting with the selection of an experimental site as close as possible to paradigmatic conditions, and a careful determination of uncertainties (which are almost always neglected in experimental studies), since turbulent fluxes under very stable conditions are so reduced that they could be significantly influenced by the characteristics of the instruments used for their determination[70]. On this point, for instance, relatively recent datasets from Arctic and Antarctic campaigns, where high levels of stability are reached and the terrain is mostly flat and homogeneous, might provide a valuable opportunity to investigate the stable and very stable SL under paradigmatic conditions[70–73]. Furthermore, the physical processes that are not considered by either MOST or EFB closure, but are expected to significantly affect the stable SL, should be carefully addressed to separate turbulent fluctuations from non-turbulent motions with larger timescales, such as internal gravity waves, Kelvin-Helmholtz shear instability, low-level jets, sub-meso motions[49,74,75]. Disentangling non-turbulent motions from turbulence requires a data analysis focused on the spectral gap that separates small-scale turbulence from mesoscale and sub-mesoscale motions. Following this approach, Howell and Sun[74] implemented a multiresolution decomposition technique to identify a turbulence cutoff time associated with the spectral gap. Their results were further extended by Vickers and Mahrt[76,77], who introduced a variable averaging time ranging from 20 min under strongly unstable to 30 s under strongly stable conditions. Nevertheless, it is important to emphasise that the development of an automatic procedure to extract the turbulent component from a generic micrometeorological signal is still an open issue.

Special attention should be paid to the possible presence of self-correlation, which is known to affect regression analysis and lead to unreliable results[12,13]. This aspect is often underestimated and, apart from the technique presented in Klipp and Mahrt[12] and Anderson[78], there are no operational strategies to assess its influence. In this respect, it is useful to mention that Anderson[78] presented a method to avoid self-correlation when determining Pr_T as a function of Ri: regression coefficients between key measurable variables are first established, and then both Pr_T and Ri are reconstructed using these relationships. The technique relies on the analysis of variance to derive both the regression and the associated error, which is used to determine the range of stability over which the technique holds.

Beyond these practical considerations, some theoretical limitations of the proposed framework should also be acknowledged. The present derivations rely on the assumption of idealised surface layer conditions, specifically, horizontal homogeneity, stationarity, and the predominance of turbulence over other motions. While such assumptions are fundamental to the MOST and EFB closures, they are not always satisfied in real atmospheric flows, particularly under very stable stratification or over heterogeneous terrain.

Recent studies[79,80] have shown that non-turbulent motions can significantly affect the structure and energy budget of the stable boundary layer. These processes may interfere with turbulence parameterisations and invalidate traditional similarity relationships.

As a result, future developments of the present framework could include the incorporation of such processes through numerical modelling or hybrid approaches. Observational campaigns targeting complex environments and using high-frequency data may also offer valuable insight into the limits of applicability of the derived universal functions. In addition to experimental campaigns, the implementation of the EFB model in high-resolution numerical simulations could help test the stability and robustness of the derived similarity functions. Similar hybrid approaches have recently been used to investigate the dynamics of complex physical systems in other domains (e.g[81]).Such simulations would allow a direct comparison between theoretical predictions and model-resolved turbulent quantities under idealised or realistic boundary-layer conditions.

Conclusions

This work demonstrates that the Energy and Flux Budget (EFB) closure framework can be used to derive definitive functional forms for all Monin-Obukhov similarity functions in the stable and very stable surface layer. By analytically linking EFB equations to the MOST framework, we provide a physically grounded and internally consistent set of similarity relationships that do not rely on empirical fitting. In addition to identifying the analytical structure of the universal functions, we establish several new constraint relationships that highlight the interdependence among these functions, an aspect often neglected in conventional analyses. These

theoretical developments contribute to a more robust understanding of turbulence in stably stratified boundary layers.

As a next step, the proposed similarity functions should be validated against comprehensive observational datasets and implemented within operational numerical models to assess their performance in realistic boundary-layer simulations.

Data availability

All data analysed during this study are included in this published article.

Received: 14 December 2024; Accepted: 7 July 2025
Published online: 15 July 2025

References

1. Monin, A. & Obukhov, A. M. Basic laws of turbulent mixing in the surface layer of the atmosphere. *Contrib. Geophys. Inst. Acad. Sci. USSR* **1954**, 163–187 (1954).
2. Edwards, J. M., Beljaars, A. C. M., Holtslag, A. A. M. & Lock, A. P. Representation of Boundary-Layer processes in numerical weather prediction and climate models. *Boundary-Layer Meteorol.* **177**, 511–539. https://doi.org/10.1007/s10546-020-00530-z (2020).
3. Falasca, S. et al. Sensitivity of near-surface meteorology to PBL schemes in WRF simulations in a port-industrial area with complex terrain. *Atmos. Res.* **264**, 105824. https://doi.org/10.1016/j.atmosres.2021.105824 (2021).
4. Tennekes, H. Similarity relations, scaling laws and spectral dynamics. *Atmos. Turbul. Air Pollut. Model A* **1981**, 37–68. https://doi.org/10.1007/978-94-010-9112-1_2 (1982).
5. Nieuwstadt, F. T. M. The turbulent structure of the stable, nocturnal boundary layer. *J. Atmos. Sci.* **41**, 2202–2216. (1984).
6. Sorbjan, Z. *Structure of the Atmospheric Boundary Layer* 317 (Wiley, 1989).
7. Stull, R. B. *An Introduction To Boundary Layer Meteorology* (Springer Netherlands, 1988).
8. Nappo, C. J. *An Introduction to Atmospheric Gravity Waves* 276 (Wiley, 2002).
9. Basu, S. et al. An inconvenient truth about using sensible heat flux as a surface boundary condition in models under stably stratified regimes. *Acta Geophys.* **56**, 88–99. https://doi.org/10.2478/S11600-007-0038-Y (2008).
10. Mortarini, L. et al. Low-frequency processes and turbulence structure in a perturbed boundary layer. *Q. J. R Meteorol. Soc.* **139**, 1059–1072. https://doi.org/10.1002/QJ.2015 (2013).
11. Mortarini, L. et al. Characterization of wind meandering in Low-Wind-Speed conditions. *Boundary-Layer Meteorol.* **161**, 165–182. https://doi.org/10.1007/S10546-016-0165-6 (2016).
12. Klipp, C. L. & Mahrt, L. Flux-gradient relationship, self-correlation and intermittency in the stable boundary layer. *Q. J. R Meteorol. Soc.* **130**, 2087–2103. https://doi.org/10.1256/QJ.03.161 (2004).
13. Grachev, A. A. et al. Stable Boundary-Layer scaling regimes: the Sheba data. *Boundary-Layer Meteorol.* **116**, 201–235. https://doi.org/10.1007/s10546-004-2729-0 (2005).
14. Casasanta, G., Sozzi, R., Petenko, I. & Argentini, S. Flux–Profile relationships in the stable boundary Layer—a critical discussion. *Atmos. (Basel).* **12**, 1197. https://doi.org/10.3390/atmos12091197 (2021).
15. Mellor, G. L. & Yamada, T. A hierarchy of turbulence closure models for planetary boundary layers. *J. Atmos. Sci.* **31**, 1791–1806 (1974).
16. Mellor, G. L. & Yamada, T. Development of a turbulence closure model for geophysical fluid problems. *Rev. Geophys.* **20**, 851–875. https://doi.org/10.1029/RG020I004P00851 (1982).
17. Yamada, T. The critical Richardson number and the ratio of the eddy transport coefficients obtained from a turbulence closure model. *J. Atmos. Sci.* **32**, 926–933 (1975).
18. Mauritsen, T. & Svensson, G. Observations of stably stratified shear-driven atmospheric turbulence at low and high Richardson numbers. *J. Atmos. Sci.* **64**, 645–655. https://doi.org/10.1175/JAS3856.1 (2007).
19. Canuto, V. M., Cheng, Y., Howard, A. M. & Esau, I. N. Stably stratified flows: a model with no Ri(cr). *J. Atmos. Sci.* **65**, 2437–2447. https://doi.org/10.1175/2007JAS2470.1 (2008).
20. Sukoriansky, S. & Galperin, B. Anisotropic turbulence and internal waves in stably stratified flows (QNSE theory). *Phys. Scr. T.* https://doi.org/10.1088/0031-8949/2008/T132/014036 (2008). T132:.
21. L'vov, V. S., Procaccia, I. & Rudenko, O. Energy conservation and second-order statistics in stably stratified turbulent boundary layers. *Environ. Fluid Mech.* **9**, 267–295. https://doi.org/10.1007/S10652-008-9117-0 (2009).
22. Khan, M. P., Chang, C-Y., Raja, M. A. Z. & Shoaib, M. Novel machine learning investigation for Buongiorno fluidic model with sutterby nanomaterial. *Tribol. Int.* **191**, 110009. https://doi.org/10.1016/j.triboint.2024.110009 (2024).
23. de Bruin, H. A. R. Analytic solutions of the equations governing the temperature fluctuation method. *Boundary-Layer Meteorol.* **68**, 427–432. https://doi.org/10.1007/BF00706800 (1994).
24. Malhi, Y. S. The significance of the dual solutions for heat fluxes measured by the temperature fluctuation method in stable conditions. *Boundary-Layer Meteorol.* **74**, 389–396. https://doi.org/10.1007/BF00712379 (1995).
25. Mahrt, L. et al. Nocturnal boundary-layer regimes. *Boundary-Layer Meteorol.* **88**, 255–278. https://doi.org/10.1023/A:1001171313493 (1998).
26. Mahrt, L. The influence of nonstationarity on the turbulent flux-gradient relationship for stable stratification. *Boundary-Layer Meteorol.* **125**, 245–264. https://doi.org/10.1007/S10546-007-9154-0 (2007).
27. Luhar, A. K. & Rayner, K. N. Methods to estimate surface fluxes of momentum and heat from routine weather observations for dispersion applications under stable stratification. *Boundary-Layer Meteorol.* **132**, 437–454. https://doi.org/10.1007/S10546-009-9409-Z (2009).
28. Wang, J. & Bras, R. L. An extremum solution of the Monin-Obukhov similarity equations. *J. Atmos. Sci.* **67**, 485–499. https://doi.org/10.1175/2009JAS3117.1 (2010).
29. van de Wiel, B. J. H. et al. Comments on an extremum solution of the monin-obukhov similarity equations. *J. Atmos. Sci.* **68**, 1405–1408. https://doi.org/10.1175/2010JAS3680.1 (2011).
30. Mauritsen, T. et al. A total turbulent energy closure model for neutrally and stably stratified atmospheric boundary layers. *J. Atmos. Sci.* **64**, 4113–4126. https://doi.org/10.1175/2007JAS2294.1 (2007).
31. Zilitinkevich, S. S. et al. On the velocity gradient in stably stratified sheared flows. Part 1: asymptotic analysis and applications. *Boundary-Layer Meteorol.* **135**, 505–511. https://doi.org/10.1007/S10546-010-9488-X (2010).
32. Li, D., Katul, G. & Zilitinkevich, S. S. Closure schemes for stably stratified atmospheric flows without turbulence cutoff. *J. Atmos. Sci.* **73**, 4817–4832. https://doi.org/10.1175/JAS-D-16-0101.1 (2016).
33. Lobocki, L. Mellor-Yamada simplified second-order closure models: analysis and application of the generalized von Karman local similarity hypothesis. *Boundary-Layer Meteorol.* **59**, 83–109. https://doi.org/10.1007/BF00120688 (1992).
34. Lobocki, L. A procedure for the derivation of surface-layer bulk relationships from simplified second-order closure models. *J. Appl. Meteorol.* **32**, 126–138 (1993).

35. Tampieri, F. Turbulence and dispersion in the planetary boundary layer. https://doi.org/10.1007/978-3-319-43604-3 (2017).
36. Zilitinkevich, S. S., Elperin, T., Kleeorin, N. & Rogachevskii, I. Energy- and flux-budget (EFB) turbulence closure model for stably stratified flows. Part I: Steady-state, homogeneous regimes. *Boundary-Layer Meteorol.* **125**, 167–191. https://doi.org/10.1007/S10546-007-9189-2 (2007a).
37. Zilitinkevich, S. S. et al. A hierarchy of Energy- and Flux-Budget (EFB) turbulence closure models for Stably-Stratified geophysical flows. *Boundary-Layer Meteorol.* **146**, 341–373. https://doi.org/10.1007/s10546-012-9768-8 (2013).
38. Kleeorin, N., Rogachevskii, I. & Zilitinkevich, S. Energy and flux budget closure theory for passive scalar in stably stratified turbulence. *Phys. Fluids*. **33**, 1–15. https://doi.org/10.1063/5.0052786 (2021).
39. Pielke, R. A. *Mesoscale Meteorological Modeling* 693 (2001).
40. Kolmogorov, A. N. Equations of turbulent motion in an incompressible fluid. *Proc. USSR Acad. Sci.* **30**, 299–303 (1941).
41. Kolmogorov, A. N. Dissipation of energy in locally isotropic turbulence. *Dokl. Akad. Nauk. SSSR*. **32**, 16 (1941).
42. Rotta, J. Statistische theorie nichthomogener turbulenz. *Z. Für Phys.* **129**, 547–572. https://doi.org/10.1007/BF01330059 (1951).
43. Schumann, U. & Gerz, T. Turbulent mixing in stably stratified shear flows. *J. Appl. Meteorol.* **34**, 33–48. https://doi.org/10.1175/1520-0450-34.1.33 (1995).
44. McMillen, R. T. An eddy correlation technique with extended applicability to non-simple terrain. *Boundary-Layer Meteorol.* **43**, 231–245. https://doi.org/10.1007/BF00128405 (1988).
45. Kaimal, J. C. & Finnigan, J. J. Atmospheric boundary layer flows. *Atmos. Bound Layer Flows*. https://doi.org/10.1093/OSO/9780195062397.001.0001 (1994).
46. Lee, X., Massman, W. & Law, B. (eds) *Handbook of Micrometeorology* (Springer Netherlands, 2005).
47. Aubinet, M., Vesala, T. & Papale, D. (eds) *Eddy Covariance* (Springer Netherlands, 2012).
48. Vickers, D. & Mahrt, L. Evaluating formulations of stable boundary layer height. *J. Appl. Meteorol.* **43**, 1736–1749. https://doi.org/10.1175/JAM2160.1 (2004).
49. Cheng, Y., Parlange, M. B. & Brutsaert, W. Pathology of Monin-Obukhov similarity in the stable boundary layer. *J. Geophys. Res. D Atmos.* **110**, 1–10. https://doi.org/10.1029/2004JD004923 (2005).
50. Asma, K., Raja, M. A. Z., Chang, C-Y., Raja, M. J. A. A. & Shoaib, M. Machine learning-driven exogenous neural architecture for nonlinear fractional cybersecurity awareness model in mobile malware propagation. *Chaos Solitons Fractals*. **179**, 115852. https://doi.org/10.1016/j.chaos.2024.115852 (2024).
51. Dyer, A. J. A review of flux-profile relationships. *Boundary-Layer Meteorol.* **7**, 363–372. https://doi.org/10.1007/BF00240838 (1974).
52. Beljaars, A. C. M. & Holtslag, A. A. M. Flux parameterization over land surfaces for atmospheric models. *J. Appl. Meteorol.* **30**, 327–341 (1991).
53. Poulos, G. S. et al. CASES-99: a comprehensive investigation of the stable nocturnal boundary layer. *Bull. Am. Meteorol. Soc.* **83**, 555–581 (2002).
54. Gryanik, V. M., Lüpkes, C., Grachev, A. & Sidorenko, D. New modified and extended stability functions for the stable boundary layer based on SHEBA and parametrizations of bulk transfer coefficients for climate models. *J. Atmos. Sci.* **77**, 2687–2716. https://doi.org/10.1175/JAS-D-19-0255.1 (2020).
55. Andreas, E. L. et al. Statistics of Surface-Layer turbulence over terrain with Metre-Scale heterogeneity. *Boundary-Layer Meteorol.* **86**, 379–408. https://doi.org/10.1023/A:1000609131683 (1998).
56. Pahlow, M., Parlange, M. B. & Porté-Agel, F. On Monin-Obukhov similarity in the stable atmospheric boundary layer. *Boundary-Layer Meteorol.* **99**, 225–248. https://doi.org/10.1023/A:1018909000098 (2001).
57. Al-Jiboori, M. H., Xu, Y. & Qian, Y. Local similarity relationships in the urban boundary layer. *Boundary-Layer Meteorol.* **102**, 63–82. https://doi.org/10.1023/A:1012745322728 (2002).
58. Quan, L. & Hu, F. Relationship between turbulent flux and variance in the urban canopy. *Meteorol. Atmos. Phys.* **104**, 29–36. https://doi.org/10.1007/S00703-008-0012-5 (2009).
59. Högström, U. et al. Turbulent exchange above a pine forest, I: fluxes and gradients. *Boundary-Layer Meteorol.* **49**, 197–217. https://doi.org/10.1007/BF00116411 (1989).
60. Hartogensis, O. K. & De Bruin, H. A. R. Monin-Obukhov similarity functions of the structure parameter of temperature and turbulent kinetic energy dissipation rate in the stable boundary layer. *Boundary-Layer Meteorol.* **116**, 253–276. https://doi.org/10.1007/S10546-004-2817-1 (2005).
61. Arya, S. P. Finite-Difference errors in Estimation of gradients in the atmospheric surface layer. *J. Appl. Meteorol.* **30**, 251–253 (1991).
62. Zilitinkevich, S. S., Elperin, T., Kleeorin, N. & Rogachevskii, I. Energy- and flux-budget (EFB) turbulence closure model for stably stratified flows. Part I: steady-state, homogeneous regimes. *Boundary-Layer Meteorol.* **125**, 167–191. https://doi.org/10.1007/s10546-007-9189-2 (2007b).
63. Zilitinkevich, S. S. et al. Turbulence energetics in stably stratified geophysical flows: strong and weak mixing regimes. *Q. J. R Meteorol. Soc.* **134**, 793–799. https://doi.org/10.1002/QJ.264 (2008).
64. Zilitinkevich, S. S. et al. Energy- and flux-budget turbulence closure model for stably stratified flows. Part II: the role of internal gravity waves. *Boundary-Layer Meteorol.* **133**, 139–164. https://doi.org/10.1007/S10546-009-9424-0 (2009).
65. Venayagamoorthy, S. K. & Stretch, D. D. On the turbulent Prandtl number in homogeneous stably stratified turbulence. *J. Fluid Mech.* **644**, 359–369. https://doi.org/10.1017/S002211200999293X (2010).
66. Zilitinkevich, S. et al. Dissipation rate of turbulent kinetic energy in stably stratified sheared flows. *Atmos. Chem. Phys.* **19**, 2489–2496. https://doi.org/10.5194/acp-19-2489-2019 (2019).
67. Högström, U. Non-dimensional wind and temperature profiles in the atmospheric surface layer: a re-evaluation. *Bound.-Layer Meteorol.* **42**, 55–78. https://doi.org/10.1007/BF00119875 (1988).
68. Chenge, Y. & Brutsaert, W. Flux-profile relationships for wind speed and temperature in the stable atmospheric boundary layer. *Bound. -Layer Meteorol.* **114**, 519–538 (2005).
69. Dias, N. L. The structure of temperature and humidity turbulent fluctuations in the stable Surface layer. PhD Thesis, Cornell University (1994).
70. Grachev, A. A. et al. Turbulent measurements in the stable atmospheric boundary layer during SHEBA: ten years after. *Acta Geophys.* **56**, 142–166. https://doi.org/10.2478/S11600-007-0048-9 (2008).
71. Casasanta, G., Pietroni, I., Petenko, I. & Argentini, S. Observed and modelled convective Mixing-Layer height at dome C, Antarctica. *Bound.-Layer Meteorol.* **151**, 523. https://doi.org/10.1007/s10546-014-9907-5 (2014).
72. Petenko, I. et al. Observations of optically active turbulence in the planetary boundary layer by Sodar at the Concordia astronomical observatory, dome C, Antarctica. *Astron. Astrophys.* **2014**, 568. https://doi.org/10.1051/0004-6361/201323299 (2014).
73. Vignon, E. et al. Momentum- and Heat-Flux parametrization at dome C, antarctica: a sensitivity study. *Boundary-Layer Meteorol.* https://doi.org/10.1007/s10546-016-0192-3 (2016).
74. Howell, J. F. & Sun, J. Surface-Layer fluxes in stable conditions. *Boundary-Layer Meteorol.* **90**, 495–520. https://doi.org/10.1023/A:1001788515355 (1999).
75. Mahrt, L., Moore, E., Vickers, D. & Jensen, N. O. Dependence of turbulent and mesoscale velocity variances on scale and stability. *J. Appl. Meteorol.* **40**, 628–641 (2001).
76. Vickers, D. & Mahrt, L. A solution for flux contamination by mesoscale motions with very weak turbulence. *Boundary-Layer Meteorol.* **118**, 431–447. https://doi.org/10.1007/s10546-005-9003-y (2006).

77. Vickers, D. & Mahrt, L. The cospectral gap and turbulent flux calculation -. *J. Atmos. Ocean. Tech.* **20**, 660–672 (2003).
78. Anderson, P. S. Measurement of Prandtl number as a function of Richardson number avoiding self-correlation. *Bound. Layer Meteorol.* **131**, 345–362. https://doi.org/10.1007/S10546-009-9376-4 (2009).
79. Stiperski, I. & Rotach, M. W. On the measurement of turbulence over complex mountainous terrain. *Boundary-Layer Meteorol.* **159**, 97–121. https://doi.org/10.1007/s10546-015-0103-z (2016).
80. Stiperski, I. & Calaf, M. Generalizing Monin–Obukhov similarity theory for complex atmospheric turbulence. *Phys. Rev. Lett.* **130**, 124001. https://doi.org/10.1103/PhysRevLett.130.124001 (2023).
81. Anwar, T. et al. Stochastic neural supervised dynamics of cholera disease under the effects of quarantine and brownian noise. *Eur. Phys. J. Plus*. **140**, 257. https://doi.org/10.1140/epjp/s13360-024-05965-8 (2025).

Author contributions

G. C. and R. S. wrote the main manuscript text and M. C. prepared Figs. 1, 2, 3, 4 and 5. A. C., I. P. and S. A. collaborated to the preparation of the draft. All authors collaborated to interpretation of results, wrote, read, commented, and approved the final manuscript.

Competing interests

The authors declare no competing interests.

Additional information

Correspondence and requests for materials should be addressed to M.C.

Reprints and permissions information is available at www.nature.com/reprints.

Publisher's note Springer Nature remains neutral with regard to jurisdictional claims in published maps and institutional affiliations.

Open Access This article is licensed under a Creative Commons Attribution-NonCommercial-NoDerivatives 4.0 International License, which permits any non-commercial use, sharing, distribution and reproduction in any medium or format, as long as you give appropriate credit to the original author(s) and the source, provide a link to the Creative Commons licence, and indicate if you modified the licensed material. You do not have permission under this licence to share adapted material derived from this article or parts of it. The images or other third party material in this article are included in the article's Creative Commons licence, unless indicated otherwise in a credit line to the material. If material is not included in the article's Creative Commons licence and your intended use is not permitted by statutory regulation or exceeds the permitted use, you will need to obtain permission directly from the copyright holder. To view a copy of this licence, visit http://creativecommons.org/licenses/by-nc-nd/4.0/.

© The Author(s) 2025